



**HAL**  
open science

# Coalescence-Controlled Anisotropic Ductile Fracture

Ahmed Amine Benzerga, Jacques Besson, André Pineau

► **To cite this version:**

Ahmed Amine Benzerga, Jacques Besson, André Pineau. Coalescence-Controlled Anisotropic Ductile Fracture. *Journal of Engineering Materials and Technology*, 1999, 121 (2), pp.221-229. 10.1115/1.2812369 . hal-03961319

**HAL Id: hal-03961319**

**<https://hal.science/hal-03961319>**

Submitted on 31 Jan 2023

**HAL** is a multi-disciplinary open access archive for the deposit and dissemination of scientific research documents, whether they are published or not. The documents may come from teaching and research institutions in France or abroad, or from public or private research centers.

L'archive ouverte pluridisciplinaire **HAL**, est destinée au dépôt et à la diffusion de documents scientifiques de niveau recherche, publiés ou non, émanant des établissements d'enseignement et de recherche français ou étrangers, des laboratoires publics ou privés.



Distributed under a Creative Commons Attribution - NonCommercial 4.0 International License

# Coalescence-Controlled Anisotropic Ductile Fracture

A. A. Benzerga

J. Besson

A. Pineau

École des Mines de Paris,  
Centre des Matériaux,  
UMR CNRS 7633, BP 87, F91003  
Evry Cedex, France

*The anisotropic ductile fracture of rolled plates containing elongated inclusions is promoted by both the dilational growth of voids and the coalescence process. In the present article, the emphasis is laid on the latter process. The effects of void shape and mainly of inter-particle spacings are investigated. Two types of coalescence models are compared: a localization-based model and plastic limit-load models. The capabilities of both approaches to incorporate shape change and spacing effects are discussed. These models are used to predict the fracture properties of two low alloy steels containing mainly manganese sulfide inclusions. Both materials are characterized in different loading directions. Microstructural data inferred from quantitative metallography are used to derive theoretical values of critical void volume fractions at incipient coalescence. These values are used in FE-calculations of axisymmetrically notched specimens with different notch radii and loading directions.*

## 1 Introduction

Modeling of ductile fracture has been essentially focused on void growth process. Constitutive models for plastic voided materials can be either based on micromechanics (Rice and Tracey, 1969; Gurson, 1977), continuum thermodynamics (Rousselier, 1987) or on variational bounds (Ponte Castaneda and Zaidman, 1994; Suquet, 1993). However, these models are unable to fully represent the actual fracture behavior of structural materials. For instance, the original Gurson model (Gurson, 1977) largely overestimates ductility. Therefore, these models were empirically modified to account not only for void growth but also for both void nucleation and coalescence. Following these approaches, coalescence is assumed to begin when a critical void growth parameter is reached (Mc Clintock, 1968). This has been successfully applied to various problems using the Rice & Tracey growth model (Rice and Tracey, 1969) together with a critical void growth ratio  $(R/R_0)_c$  (Beremin, 1981; Lautridou and Pineau, 1981; Marini et al., 1985). Similarly, (Tvergaard and Needleman, 1984) used the Gurson model together with a critical porosity  $f_c$ . These critical parameters were initially considered as material constants. Recent theoretical and numerical results (Koplik and Needleman, 1988; Perrin, 1992; Zhang and Niemi, 1994; Brocks et al., 1995) indicate that  $f_c$  could be a function of the stress state as previously evidenced in (Lautridou and Pineau, 1981). Moreover, arises the question of the role of evolving microstructure, mainly void spacing and void shape, on the coalescence at a given stress state. Experimental investigations on void coalescence (see e.g. (Garrison and Moody, 1987a)) showed that, at least, two micromechanisms, void impingement or void-sheet process, could lead to the final stage of dimpled fracture. In particular, inclusion distribution has been shown to strongly influence the fracture toughness of metals (Garrison and Moody, 1987b) for a given volume fraction of inclusions.

In the present study, the emphasis is laid on the determination of  $f_c$  as a function of stress state and the above microstructural parameters. The calculated values are then used in a Gurson-like model following (Tvergaard and Needleman, 1984). It is believed that, using this approach,  $f_c$  can be determined from measured microstructural data, instead of being fitted from experimental macroscopic load—displacement responses. Void

coalescence by void-sheet mechanism has been theoretically analyzed in (Leblond and Perrin, 1991). Thomason (Thomason, 1985b) used a quite different approach in which coalescence is the result of necking down of the intervoid matrix. The critical porosity is derived from both models as being a function of stress triaxiality.

The present paper first reviews the different micromechanical models for coalescence. Their ability to incorporate void shape and spacing is discussed. The models are then applied to predict the anisotropic fracture of two hot worked steels containing large manganese sulfide inclusions elongated along the primary working direction. Such steels exhibit a strong anisotropic behavior of both plastic flow and ductility. Finite element calculations were performed to model the behavior of notched specimens. The constitutive equations are based on a Gurson-like model which incorporates plastic anisotropy (Doege et al., 1995; Benzerga et al., 1997). Critical void volume fraction for the onset of coalescence is based on the previous models as a function of stress triaxiality ratio and the mean particle spacing.

## 2 Coalescence Modeling

The growth of spherical voids can be described by the widely used Gurson model. This model is defined by a plastic potential  $\Phi(\Sigma, f)$  together with an evolution law of the damage parameter, namely the porosity  $f$ , according to:

$$\Phi(\Sigma, f) = (X(f))^2 + 2qf \cosh\left(\frac{3}{2}\mathcal{F}X(f)\right) - 1 - (qf)^2 = 0 \quad (1)$$

$$\frac{df}{d\epsilon_{eq}} = \frac{3}{2}q \frac{f(1-f)}{X(f)} \sinh\left(\frac{3}{2}\mathcal{F}X(f)\right) \quad (2)$$

where  $X = \Sigma_{eq}/\sigma_y$ ,  $\Sigma_{eq}$  being the macroscopic equivalent stress and  $\sigma_y$  the yield stress of the sound material;  $\mathcal{F} = \Sigma_m/\Sigma_{eq}$  is the stress triaxiality ratio,  $\Sigma_m$  the hydrostatic stress and  $q$  a coefficient reflecting void interactions (Tvergaard, 1981). Equation (2) is deduced from mass conservation and the macroscopic normality rule.  $\epsilon_{eq}$  is the macroscopic equivalent plastic strain.

It is worth emphasizing that the Gurson model, as many others, is not a fully predictive approach to fracture. These models describe the overall behavior of a voided solid. Purely empirical coalescence modeling was attempted (Tvergaard and Needleman, 1984) in order to incorporate some failure criterion in the Gurson model, by assuming an effective porosity  $f^*$

which reflects increasing cavitation after the onset of coalescence.

In this section, we are interested in predictive models of the onset of coalescence. Two types of models, based on a priori different concepts, are considered. The first one considers the coalescence as a bifurcation behavior in a pressure-sensitive material. The second type of model is also based on an instability condition which expresses that coalescence occurs by a plastic limit-load mechanism in the ligament between cavities.

To assess the ability of each type of models to incorporate void shape effects, a recently proposed micromechanical model accounting for void shape evolution (Gologanu et al., 1994; Gologanu et al., 1995) was used. This model provides constitutive equations of transversely isotropic porous plastic materials containing aligned spheroidal voids and subject to axisymmetric loading conditions. The model does not accurately account for cavity rotation in off-axes tension for which the principal stresses are not aligned with the symmetry axes (Benzerga et al., 1997).

The model is formulated in terms of a Gurson-like plastic potential  $\Phi_w$ :

$$\Phi_w(\Sigma, f, W) = C \frac{\|\Sigma' + \eta \Sigma_h \mathbf{X}\|^2}{\sigma_y^2} + 2q_w(g+1)(g+f) \times \cosh\left(\frac{\kappa \Sigma_h}{\sigma_y}\right) - (g+1)^2 - q_w^2(g+f)^2 \quad (3)$$

with

$$\Sigma_h = \alpha_2(\Sigma_{11} + \Sigma_{22}) + (1 - 2\alpha_2)\Sigma_{33} \quad (4)$$

$\sigma_y$  is the matrix flow stress,  $\Sigma'$  the deviatoric part of  $\Sigma$ ,  $\|\cdot\|$  the von Mises norm,  $\Sigma_h$  a weighted average of the principal stresses,  $\mathbf{X}$  a constant tensor, and  $C, \eta, g, \kappa$  and  $\alpha_2$  are coefficients which depend only on the porosity  $f$  and the void aspect ratio  $W$  defined hereafter while  $\alpha_1, \alpha_1^c$  and  $q_w$  depend on  $W$  only. The third direction corresponds to the common axis of the voids. The evolution law of  $f$  is derived using mass conservation and macroscopic normality as in the original Gurson model. Denoting  $\mathbf{D}$  the plastic strain rate tensor and  $\mathbf{D}'$  its deviator, the evolution of the void aspect ratio is governed by:

$$\frac{\dot{W}}{W} = \frac{3}{2} \left[ 1 + \frac{3}{2} h_{\mathcal{T}}(\mathcal{T})(1 - \sqrt{f})^2 \frac{\alpha_1 - \alpha_1^c}{1 - 3\alpha_1} \right] D'_{33} + 3 \left( \frac{1 - 3\alpha_1}{f} + 3\alpha_2 - 1 \right) D_m \quad (5)$$

where  $D_m$  and  $D'_{33}$  are the mean part of  $\mathbf{D}$  and the  $\mathbf{D}'$ -component parallel to voids respectively. See (Gologanu et al., 1995) for full expressions of  $W$ -functions and  $h_{\mathcal{T}}(\mathcal{T})$ .

Preliminary studies using this model for different proportional stress states and initial void aspects ratios are presented elsewhere (Benzerga et al., 1998).

**2.1 Localization-Based Coalescence Model.** Constitutive models for plastic porous metals (Gurson, 1977; Rousselier, 1987) are primarily attractive for their capability to be used in strain-localization analyses. Attempt was made (Yamamoto, 1978) to investigate the theory of the localization of deformation in dilatant materials (Rudnicki and Rice, 1975) in the case of a Gurson material. Predictions of ductility were, however, well in excess in comparison with experimental values (Edelson and Baldwin, 1962). The previous approach suffers from considering an homogeneous distribution of voids during deformation. Experimental observations (Pineau, 1981) have shown however that void distribution becomes anisotropic due to deformation. Pursuing this idea and considering a doubly periodic

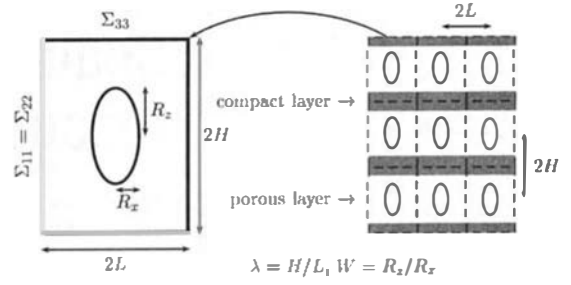


Fig. 1 Axisymmetric Unit-cell

array of voids (Fig. 1), Leblond and Perrin (Leblond and Perrin, 1991) (see also (Perrin, 1992)) proposed a coalescence criterion with the following assumptions: ( $\mathcal{A}_1$ ) Axisymmetric loading conditions are assumed (Fig. 1). The stress state is then proportional and characterized by the triaxiality  $\mathcal{T}$ . It is then useful to write the macroscopic stresses:  $\Sigma_{33}/\sigma_y = (\mathcal{T} + \frac{2}{3})X$  and  $\Sigma_{11}/\sigma_y = (\mathcal{T} - \frac{1}{3})X$ . In this analysis, one assumes that  $\Sigma_{33} > \Sigma_{11}$ . The geometry is described by three dimensionless parameters, the porosity  $f$ , the particle-spacing ratio  $\lambda = H/L$  and the void aspect ratio  $W = R_z/R_x$  (Fig. 1). ( $\mathcal{A}_2$ ) Perfect plasticity is assumed for the matrix behavior. ( $\mathcal{A}_3$ ) At a macroscopic scale, the stress state  $(\Sigma_{11}, \Sigma_{33})$  lies on the Gurson yield surface, Eq. (1). ( $\mathcal{A}_4$ ) Coalescence arises from the progressive concentration of voids in some layers separated by compact regions, Fig. 1. This introduces the concept of a deformation-induced heterogeneity. Coalescence occurs when the localization condition (Rudnicki and Rice, 1975) is fulfilled in the porous layers which correspond to the mesoscopic scale of the model.

It is worth noting that ( $\mathcal{A}_2$ ) is not restrictive since strain hardening has little effect on critical porosities (Perrin, 1992). Assumption ( $\mathcal{A}_4$ ) introduces the concept of a local porosity,  $f_p$ , that of the highly porous layers. In order to evaluate  $f_p$ , Perrin (Perrin, 1992) assumed that voids are isotropically distributed when stacking the highly porous layers, which leads to  $f_p = f\lambda$  (see Fig. 1).  $\lambda$  is the current height to radius ratio of the unit-cell (Fig. 1). ( $\mathcal{A}_4$ ) enforces the localization to occur in a horizontal plane such that no prediction of the localization direction is done. To write the localization condition, we introduce the mesoscopic stresses in the porous layers  $\Sigma_{11}^{(p)} = \Sigma_{22}^{(p)}$  and  $\Sigma_{33}^{(p)} = \Sigma_{33}$  (axial equilibrium). Let  $\gamma = \Sigma_{11}^{(p)}/\sigma_y$  and  $sh$  and  $ch$  the hyperbolic sine and cosine of  $(\frac{1}{2}(\mathcal{T} + \frac{2}{3})X(f) + \gamma)$ .

The porous layer is plastically deforming so that the local stress tensor  $\Sigma_{ij}^{(p)}$  obeys the Gurson criterion written using the local porosity  $f^{(p)}$ :

$$\Phi(\Sigma^{(p)}, f^{(p)}) = ((\mathcal{T} + \frac{2}{3})X(f) - \gamma)^2 + 2qf^{(p)}ch - 1 - q^2(f^{(p)})^2 = 0 \quad (6)$$

The coalescence condition then writes (Perrin, 1992):

$$3(1 - \nu) \frac{\sigma_y}{E} q^2(1 - f^{(p)})f^{(p)}sh(ch - qf^{(p)}) = ((\mathcal{T} + \frac{2}{3})X(f) - \gamma - qf^{(p)}sh)^2 \quad (7)$$

In the case of metallic materials  $\sigma_y/E$  is small, so that the left-hand side of the previous equation can be neglected. In that case, the localization condition expresses the fact that the lateral flow rate in the plastically deformed layer is equal to zero. This is consistent with the fact that the sound layers become rigid.

As a summary, coalescence occurs when condition (7) is observed with respect to Eqs. (1) and (2) for the macroscopic behavior and Eq. (6) for the mesoscopic behavior. The localization based model described above is referred to as model ( $\mathcal{L}$ ) in the sequel.

Finally, as far as the incorporation of void shape in the previous localization framework is concerned, one should note that the yield surfaces derived from (Gologanu et al., 1995), Eq. (3) are not isotropic. The use of the Rudnicki and Rice's analysis is then no longer appropriate. The analysis extending that work to anisotropic materials, due to Ottosen and Runesson (Ottosen and Runesson, 1991), increases the complexity of the model and hence is not addressed in the present study.

**2.2 Plastic Limit-Load Coalescence Models.** The second model (Thomason, 1968; Thomason, 1985b) assumes that coalescence initiates when the intervoid ligament reaches its plastic limit-load. At this stage plastic flow becomes highly localized. Unit cell calculations (Koplik and Needleman, 1988) gave further support to Thomason's ideas. The coalescence condition can then be easily written by considering the equilibrium of the ligament (see Fig. 1):

$$\pi(L^2 - R_x^2)\mathcal{C}_f\sigma_y = \pi L^2\Sigma_{33} \quad (8)$$

The force in the loading direction expressed in the ligament region (left-hand side) must be equal to the force applied on the cell boundary (right hand-side). The cavity induces a stress concentration in the ligament thus increasing the ligament stress triaxiality. The load-carrying capacity of the ligament is therefore increased. This effect is described by the plastic constraint factor  $\mathcal{C}_f$  in the previous equation. In the case of the axisymmetric cell depicted on Fig. 1,  $\mathcal{C}_f$  can be derived using the upper-bound theorem for limit-load analysis (Thomason, 1985b):

$$\begin{aligned} \mathcal{C}_f &= 0.1 \left( \frac{R_z}{L - R_x} \right)^{-2} + 1.2 \left( \frac{R_x}{L} \right)^{-1/2} \\ &= 0.1 \left( \frac{L/R_x - 1}{W} \right)^2 + 1.2\sqrt{L/R_x} \end{aligned} \quad (9)$$

with  $W = R_z/R_x$ . Noting that  $\Sigma_{33} = (\frac{2}{3} + \mathcal{T})\Sigma_{eq}$ , the coalescence condition is expressed as:

$$A_n\mathcal{C}_f = (\frac{2}{3} + \mathcal{T})X(f) \quad \text{with} \quad A_n = 1 - \frac{R_x^2}{L^2} \quad (10)$$

$A_n$  is the matrix area fraction in the loading direction and  $X(f)$  is still defined as the ratio  $\Sigma_{eq}/\sigma_y$ . Thomason's criterion for coalescence is purely based on geometrical considerations. It can then be applied noting that:

$$\frac{R_x}{L} = \left[ \frac{3}{2} \frac{f}{W} \lambda \right]^{1/3} \quad (11)$$

where  $\lambda = H/L$  can be derived from the macroscopic deformation and the initial value  $\lambda_0$ . Evolution of porosity, void shape and remote stress field  $\Sigma_{ij}$  must be derived using an appropriate model to apply the coalescence criterion.

The model, referred to as ( $\mathcal{P}L1$ ), was first applied assuming (Thomason, 1985a): ( $\mathcal{A}_2$ ) perfect plasticity, ( $\mathcal{A}_5$ ) that voids are initially spherical, ( $\mathcal{A}_6$ ) that the porosity remains constant, ( $\mathcal{A}_7$ ) that the overall behavior is obtained applying the law of mixture  $\Sigma_{eq} = (1 - f)\sigma_y$  or  $X(f) = 1 - f$ . These assumptions are the consequence of the use of a void growth model for isolated voids (Rice and Tracey, 1969) assuming incompressibility. In addition, the cavity shape change was accounted for by Thomason using an integration of the Rice and Tracey equations.

However, this model has two major drawbacks: (1) At low triaxialities  $\mathcal{T} < 1$  and for porosities frequently observed in steels (i.e.,  $< 0.1\%$ ), unrealistically high ductilities are found (see Thomason, 1985a). This is essentially due to the fact that the material is assumed to be incompressible. (2) At high porosities or high triaxialities, the law of mixture underestimates the

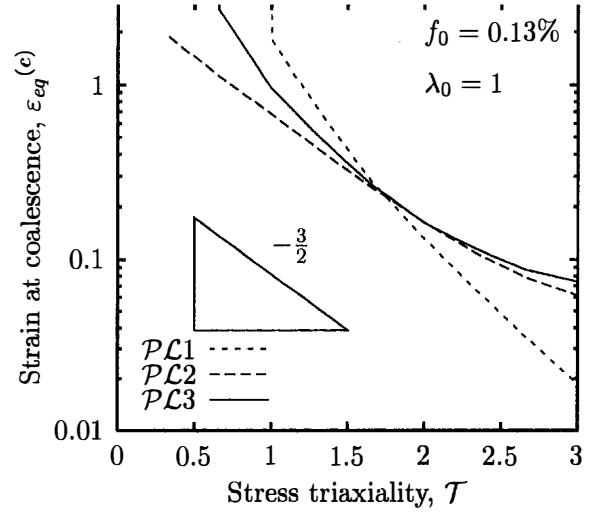


**Fig. 2 Numerical results using plastic limit load models: ( $\mathcal{P}L1$ ) original model of Thomason (Thomason, 1985a), ( $\mathcal{P}L2$ ) accounting for compressibility (Zhang and Niemi, 1994), ( $\mathcal{P}L3$ ) accounting for void shape effect (this paper). Equivalent strain-Triaxiality curves.**

net decrease of the macroscopic equivalent stress, see e.g., Koplik and Needleman (1988). This leads to an underestimation of the ductility. It is worth mentioning that a variant of model ( $\mathcal{P}L1$ ) has been used to predict the failure of copper notched bars (Pardo et al., 1998). This version still contains some of the drawbacks mentioned above because of the implicit assumption of incompressibility.

In order to overcome these drawbacks, Zhang and Niemi (Zhang and Niemi, 1994) used the Gurson model to compute both  $f$  and  $X(f)$ , from Eqs. (1) and (2), as a function of the load history characterized by  $\mathcal{T}$ . The limit-load criterion Eqs. (9) to (11), is then used (model ( $\mathcal{P}L2$ )). In that case, due to the use of the isotropic Gurson model, cavities are necessarily assumed to be initially and to remain spherical ( $W = R_z/R_x = 1$ ).

Alternatively, a new and original approach is proposed. Void shape effects are fully accounted for using the constitutive model defined by Eqs. (3) and (5). The limit-load criterion is then applied without any approximation on the void shape. This approach, ( $\mathcal{P}L3$ ), is used in order to emphasize the role of void shape in the coalescence modeling.

### 3 Theoretical Fracture Strains and Porosities

The aim of this section is first to present numerical results for a wide range of stress triaxiality ratios and initial void volume fractions, using the four above models. Then, the effect of initial void spacing, characterized in axisymmetric configurations by a single parameter  $\lambda_0$ , is also investigated. For that purpose, the sets of equations (1, 2, 6, 7) for model ( $\mathcal{L}$ ) and (1, 2, 9, 10, 11) for models ( $\mathcal{P}L1$ ) and ( $\mathcal{P}L2$ ) were solved numerically using the MAPLE software. Finally, some preliminary results obtained using the new model ( $\mathcal{P}L3$ ) accounting for void shape effect are presented. All calculations based on the Gurson model were made with  $q = 1.35$ . This value was selected in order to compare the present results with published data (Leblond and Perrin, 1991). Commonly used values of  $q$  range from 1 to 1.6. It was checked that the presented trends are independent on the selected value.

**3.1 Comparison of the Plastic Limit-Load Models.** Figure 2 illustrates the first drawback of the original Thomason's model ( $\mathcal{P}L1$ ) for triaxialities between  $\frac{1}{3}$  and 3 and  $f_0 = 0.13\%$  which is commonly used in unit-cell calculations. Accounting for compressibility improves results at low triaxialities for which model ( $\mathcal{P}L1$ ) predicts infinite ductilities. On the other

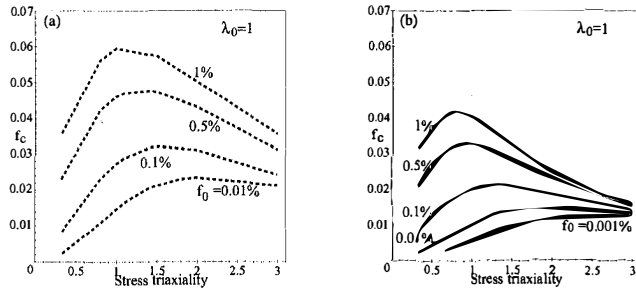


**Fig. 3 Critical porosity—Triaxiality curves using (a) model ( $\mathcal{L}$ ) and (b) model ( $\mathcal{PL2}$ )**

hand, at high triaxialities or high initial porosities, ( $\mathcal{PL2}$ ) predicts a higher ductility. This is due to a larger decrease of the macroscopic stress  $\Sigma_{eq}$  so that the load on the intervoid ligament is smaller thus preventing early coalescence. Note that ( $\mathcal{PL1}$ ) assumes that  $\Sigma_{eq}$  remains constant as the porosity is not changing. This improvement, due to accounting for compressibility, is actually questionable since a spherical void growth is assumed. One should however notice that for the intermediate triaxiality  $\mathcal{T} = 1.5$ , initially spherical voids do grow spherically without shape change, see for instance Budiansky et al. (1982) and Koplik and Needleman (1988). Hence for that triaxiality, the evolution of the void is exactly described by the Gurson constitutive model. It is then concluded that the obtained results are not an artefact that may be due to a poor description of void shape change, but essentially due to accounting for compressibility.

A more accurate description of void shape effect is provided by model ( $\mathcal{PL3}$ ). Ductilities assessed from this model are also indicated on Fig. 2. At low triaxiality ( $\mathcal{T} < 1$ ), the new model gives intermediate ductilities. This is due to the fact that: (1) spherical voids tend to become prolate thus increasing the ductility (Benzerga et al., 1998) in comparison with ( $\mathcal{PL2}$ ); (2) the evolution of the porosity is accounted for, thus leading to more realistic ductilities in comparison with ( $\mathcal{PL1}$ ). For  $\mathcal{T} = \frac{1}{3}$ , it is worth noting that coalescence does not occur, which is consistent with recent unit cell calculations (Gologanu, 1997). Therefore, the use of model ( $\mathcal{PL2}$ ) (which neglects shape change effect) leads to a wrong result for that triaxiality. Note that smooth tensile bars ( $\mathcal{T} = \frac{1}{3}$ ) usually fail after necking, which locally increases the stress triaxiality.

In Fig. 2, we can compare the calculated curves with a straight line of slope  $-\frac{3}{2}$ . This value is easily found from the application of growth models (Rice and Tracey, Gurson) assuming that fracture occurs for a constant critical void growth ratio. The results given in Fig. 2 clearly indicate that this assumption does not apply for all values of stress triaxiality.

### 3.2 Comparison of Localization, And Limit Load, Based Models

**3.2.1 Effect of Inclusion Volume Fraction.** Numerical integration of the equations of model ( $\mathcal{L}$ ) for  $\mathcal{T} = 1, 2$  and 3 (Perrin, 1992) has shown a very good agreement with results obtained from unit-cell calculations (Koplik and Needleman, 1988). Further results are shown in Fig. 3(a), for a wide range of  $f_0$  values in an initially isotropic material ( $\lambda_0 = 1$ ). Critical porosities are plotted against stress triaxiality. A similar set of curves obtained using model ( $\mathcal{PL2}$ ) is shown in Fig. 3(b).

The general trend is the same for both models. For a given material ( $f_0, \lambda_0$ ), the critical porosity—stress triaxiality curve delimits a domain in which coalescence cannot occur. Each curve exhibits a maximum reached for a value of triaxiality,  $\mathcal{T}_i$ , dependent on  $f_0$ .  $\mathcal{T}_i$  increases when the material becomes “cleaner” (i.e., for low  $f_0$ ).

One should note that  $f_c$ -values deduced from ( $\mathcal{PL2}$ ) are somewhat lower than those predicted from ( $\mathcal{L}$ ), thus leading

to relatively lower predicted ductilities. Note also that for highly clean materials (for instance, for high strength steels containing MnS inclusions, with  $\%S < 20$  ppm, i.e.,  $f_0 < 0.01\%$ ), the onset of coalescence is almost independent on the stress state for  $\mathcal{T} > 1.5$ .

**3.2.2 Effect of Void Spacing.** Initial void spacing effect is illustrated in Fig. 4 where predictions from both approaches ( $\mathcal{L}$ ) and ( $\mathcal{PL2}$ ) are compared. There is actually a difference in predicted  $f_c$  values between ( $\mathcal{L}$ ) and ( $\mathcal{PL2}$ ) models even though the difference becomes less significant for high values of  $\lambda_0$ . But the main feature evidenced in Fig. 4 remains the drastic effect of void distribution on ductility according to both models. This result suggests that the macroscopically observed anisotropic fracture of rolled plates for instance, may be partly due to an anisotropic distribution of particles nucleating voids. Moreover, Fig. 4 shows that the asymptotic critical porosity value, reached at high triaxialities, and observed in Fig. 3 (b) is dependent only on the initial distribution of voids  $\lambda_0$ . The  $f_c$  limit value decreases with increasing  $\lambda_0$  (Fig. 4).

**3.3 Effect of Void Shape.** The aim of this part is first to determine the corrections that may be brought by the incorporation of void shape change to the results predicted by model ( $\mathcal{PL2}$ ). It is then to study, within a representative stress state range, the effect of the initial void shape on strains and porosities at coalescence.

This study is made possible using the constitutive model incorporating void shape effects (Gologanu et al., 1995) together with the plastic limit-load coalescence criterion. This model was implemented (Benzerga et al., 1998) in the finite element code ZéBuLoN7 (Besson and Foerch, 1997). Details of the finite element implementation will be given elsewhere. The coalescence model has also been implemented as a post-processor. This implementation allows for a continuous evaluation of the coalescence criterion with evolving stress, strain and microstructural parameters  $f$  and  $W$ .

A series of calculations have been performed on a representative volume element. In order to keep a given stress triaxiality ratio, the stress state was controlled using Riks’ algorithm (Riks, 1979).

**3.3.1 Initially Spherical Voids.** We begin first with a comparison between a model that neglects void shape change, ( $\mathcal{PL2}$ ), and the new model ( $\mathcal{PL3}$ ). For that purpose, two extreme initial porosities  $f_0 = 1\%$  and  $f_0 = 0.001\%$  are consid-

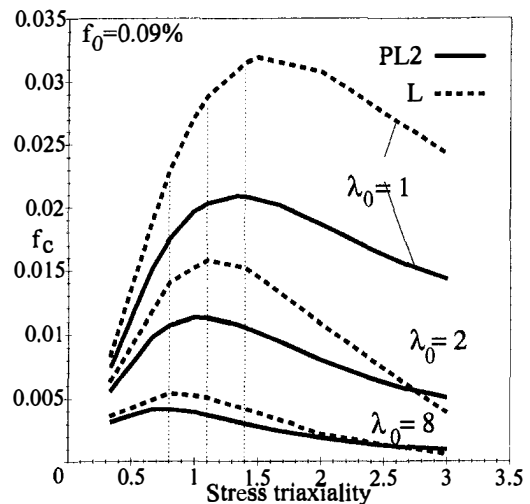


**Fig. 4 Critical porosity—Triaxiality curves for various initial void distributions**

**Table 1 Void shape effect on predicted  $\epsilon_{eq}^{(c)}$  and  $f_c$  for initially spherical voids,  $W_0 = 1$ .  $q = 1.35$**

Coalescence parameters	$\mathcal{T} = 2/3$		$\mathcal{T} = 1$		$\mathcal{T} = 4/3$		$\mathcal{T} = 3$	
	$f_0 = 1\%$	$0.001\%$	$f_0 = 1\%$	$0.001\%$	$f_0 = 1\%$	$0.001\%$	$f_0 = 1\%$	$0.001\%$
(PL3)								
$f_c(\%)$	11.1	0.95	8.16	1.30	5.0	1.34	1.6	1.40
$\epsilon_{eq}^{(c)}$	1.75	5.34	0.629	1.87	0.29	0.97	0.02	0.09
(PL2)								
$f_c(\%)$	4.21	0.26	4.22	0.57	3.75	0.91	1.76	1.36
$\epsilon_{eq}^{(c)}$	0.627	2.34	0.357	1.48	0.204	0.93	0.024	0.11

ered. The obtained results for various stress triaxialities are gathered in Table 1.

As mentioned above, no coalescence is predicted by the new model for a triaxiality of  $\frac{1}{3}$ . Classical approaches similar to (PL2) give a wrong prediction because they still consider that void growth is governed by the mean stress since they assume that voids grow spherically. The explanation of this particular behavior for  $\mathcal{T} = \frac{1}{3}$ , is that voids elongate along the principal straining direction and tend to become cylindrical ( $W \rightarrow \infty$ ). Since the growth of cylindrical voids is governed by the mean lateral stress (Mc Clintock, 1968; Gurson, 1977), which is equal to zero in uniaxial tension, porosity remains constant. As a consequence, the coalescence condition (10) is no longer reached. More generally, the influence of void shape change seems, as expected, to be significant at low triaxiality  $\mathcal{T} < \frac{4}{3}$ . By assuming spherical void growth, model (PL2), one underestimates both the critical porosity and the strain at coalescence. However, for a triaxiality  $\mathcal{T} \approx 3$  frequently encountered at a blunted crack tip in plane strain conditions, the evolution of void shape has little effect.

**3.3.2 Effect of Initial Void Shape.** As an extension of the finite element simulations of unit-cells containing spherical voids (Koplik and Needleman, 1988; Brocks et al., 1995; Gologanu, 1997), Sovik and Thaulow (1997) performed analogous simulations with different initial void aspect ratios ranging from  $W_0 = \frac{1}{3}$  to  $W_0 = 3$ , and an initial porosity of 0.02%. Two stress triaxialities were considered  $\mathcal{T} = 1$  and  $\mathcal{T} = \frac{8}{3}$ . These simulations are a reference to investigate the ability of the new model (PL3) to correctly predict the onset of coalescence. Our predictions are given using a  $q$  parameter of 1.6. This value was recommended in the use of the constitutive model incorporating void shape effects (Gologanu, 1997). Table 2 shows the comparison between the predictions of model (PL3) and the unit-cell results. For  $\mathcal{T} = 1$ , a small increase in predicted  $f_c$ -values with  $W_0$  is observed, whereas results of Sovik and Thaulow (Sovik and Thaulow, 1997) suggest a moderate decrease of  $f_c$ . This small difference may be due to the difficulty to determine the porosity value when coalescence occurs in the cell calculations. It is worth noting the excellent correspondance between the macroscopic equivalent strains at coalescence. This is obtained without any adjustment of the model parameters.

Further results are presented in Fig. 5 for a wider range of initial void aspect ratio  $W_0$ . Three triaxiality values are considered:  $\mathcal{T} = 0.8$  and  $\mathcal{T} = \frac{4}{3}$  that prevail in moderately (severely, resp.) notched bars and  $\mathcal{T} = \frac{10}{3}$  for a crack tip. At high triaxiality, it appears that the effect of inclusions morphology is negligible, whereas the influence of inclusions spacing is not. At  $\mathcal{T} = 0.8$  however, a net increase in the strain at coalescence with  $W_0$  is observed for both values of the inclusion spacing ratio.

**Table 2 Coalescence parameters  $\epsilon_{eq}^{(c)}$  and  $f_c$  for various initial shapes. Comparison between unit-cell FE-calculations (Sovik and Thaulow, 1997) and our model with  $q = 1.6$ .**

Coalescence parameters	$\mathcal{T} = 1$			$\mathcal{T} = 8/3$		
	$W_0 = 1/3$	$W_0 = 1$	$W_0 = 3$	$W_0 = 1/3$	$W_0 = 1$	$W_0 = 3$
(PL3)						
$f_c(\%)$	3.0	3.2	3.5	2.0	1.82	2.1
$\epsilon_{eq}^{(c)}$	0.995	1.14	1.38	0.109	0.102	0.112
Sovik						
$f_c(\%)$	2.5	1.9	1.75	-	-	-
$\epsilon_{eq}^{(c)}$	0.92	1.08	1.35	0.115	0.12	0.11

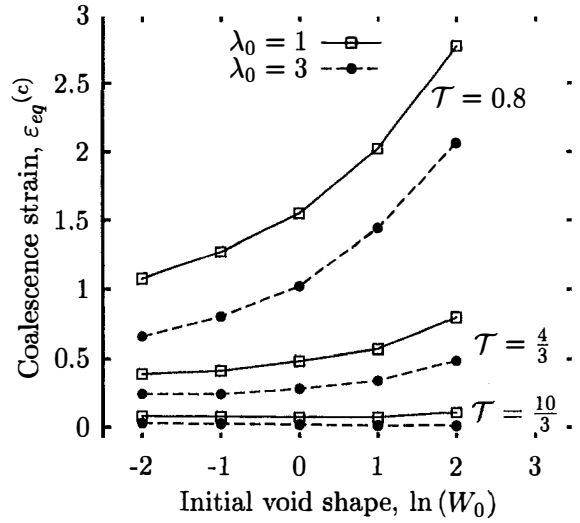


**Fig. 5 Equivalent plastic strain at coalescence  $\epsilon_{eq}^{(c)}$  versus initial void shape  $W_0$  for various stress states and two inclusion spacing ratios**

## 4 Application

### 4.1 Experiments

**Materials.** Two materials were investigated. The first one, labeled **A**, is a ferritic-pearlitic steel of grade X52 cut from a rolled sheet of 10 mm thickness. The main elements of the chemical composition are (C = 0.17, S = 0.009, Mn = 1.23, Nb = 0.0038 wt%). The second material, **B**, is a forged A508 steel (C = 0.15, S = 0.010, Mn = 1.47, Al = 0.029 wt%) used in nuclear pressure vessel construction (Lautridou and Pineau, 1981). Its microstructure is essentially tempered bainite. Both materials were given different hot working schedules leading to different anisotropic behavior. These materials contain similar amounts of sulfur and manganese. Steel **A** exhibits an anisotropic plastic flow whereas **B** is isotropic. **A** and **B** also differ in the morphology of MnS inclusions they contain. Of interest are both materials since MnS particles have a low interfacial strength, thus nucleating voids at very low strains. This allows to circumvent some of the problems related to void nucleation (Beremin, 1981) and to concentrate on issues of void growth and coalescence. In the following,  $L$  will denote the primary working direction which is either the rolling direction (steel **A**) or the longitudinal forging direction (steel **B**),  $T$  and  $S$  the transverse and the short transverse directions respectively.  $L$ ,  $T$  and  $S$  represent the three principal directions of orthotropy of material **A**.  $LT$  corresponds to the orientation at 45 deg to  $L$ -axis in  $L$ - $T$  plane. The tensile properties of both materials are summarized in Table 3.

**Inclusion Characterization.** High resolution optical microscope images of polished sections taken at 1000 $\times$  were analyzed to determine the inclusion volume fraction and mean inclusion dimensions. For both materials, the observed plane sections, denoted ( $L$ ), ( $T$ ) and ( $S$ ), were perpendicular to the three principal directions of the materials,  $L$ ,  $T$  and  $S$  respectively. Most of the observed inclusions were elongated MnS particles. In steel **A**, some Niobium carbides of size lying between 0.1

**Table 3 Tensile properties and mean strains to failure ( $\bar{\epsilon}_f$ ) in notched bars**

Steels	Tensile axis	Yield Stress (MPa)	Ultimate Strength (MPa)	Fracture strain (%)	$\bar{\epsilon}_f$ (AER) (%)		
					10	4	2
<b>A</b>	L	405	532	120	88.5	67.5	52.8
	T	370	540	96	55.7	36.9	26.0
	LT	420	525	128	89.0	58.5	45.5
<b>B</b>	L	466	590	126	70.0	48.0	30.0
	S	476	595	74	28.4	16.0	12.0

**Table 4 Quantitative metallography.** (\*) refers to MnS only; (\*\*) data taken from (Lautridou and Pineau, 1981)

Steel	$\mathcal{A}_a$ ( $\mu\text{m}^2/\text{mm}^2$ )			$f_a$ (%)	$V_v$ (%)	$D_L$ ( $\mu\text{m}$ )	$D_T$ ( $\mu\text{m}$ )	$D_S$ ( $\mu\text{m}$ )	$f_v$ (%)
	(L)	(T)	(S)						
<b>A</b>	364	1069	425	.06	0.047	44.3*	10.7	2.6	0.09
<b>B**</b>	386	624	703	.057	0.050	15*	10	5	0.04

$\mu\text{m}$  and  $5 \mu\text{m}$  were also observed. In addition to MnS particles, steel **B** contained also a small amount of tiny oxides. Both carbides and oxides differ from MnS inclusions in both size and shape. They are spherical as they do not deform during hot working.

Only particles greater than  $2 \mu\text{m}$  were analyzed. The volume fraction was determined using the methodology followed by others (Mudry, 1982; Batisse et al., 1988). The results are summarized in Table 4. The mean area fraction  $f_a$ , averaged from the values of the inclusion surface per unit area in each plane,  $\mathcal{A}_a$ , can be compared to the volume fraction,  $V_v$ , inferred from the chemical composition using Franklin's relationship (Franklin, 1969). Average 3D dimensions,  $D_i$ , and the volume fraction of inclusions,  $f_v$ , were determined by stereological formulae, see Lautridou and Pineau (1981). On this basis, it is noted that the voids associated with MnS inclusions of steel **A** are more elongated than those in steel **B**.

**Ductility Measurement on Notched Bars.** In order to study ductility anisotropy in proportional loading conditions, tensile tests on axisymmetric notched bars, cut in several orientations, were carried out. These samples are labeled AER $\chi$  with  $\chi$  being equal to ten times the ratio of the notch radius to the nominal minimum diameter. Three geometries corresponding to three different notch radii were used. The most severely notched specimen, AER2, exhibits the higher stress triaxiality. For each test, both principal diameters in the minimal section,  $\Phi_1$  and  $\Phi_2$ , were measured.  $\Phi_1$  was the actual diameter along the short transverse direction  $S$ . The mean strain is defined as:  $\bar{\epsilon} = \ln(\Phi_0^2/(\Phi_1\Phi_2))$ , where  $\Phi_0$  is the initial diameter. Mean strains to failure  $\bar{\epsilon}_f$  are reported in Table 3. For steel **A**, it is worth noting that the decrease in  $\bar{\epsilon}_f$  with increasing stress triaxiality is much slower for  $L$ -loading than for  $T$ - or  $LT$ -loading. On the other hand, the comparison between **A** and **B** shows that (1) **A** is more ductile than **B** and (2) in  $L$ -loading, the decrease in ductility with stress triaxiality for steel **B** is more rapid. For instance,  $\bar{\epsilon}_f$  in AER10 specimens is more than twice higher in comparison with  $\bar{\epsilon}_f$  in AER2 specimens. These results can be explained by the synergistic effects of both inclusion spacing and inclusion shape.

**Observations.** In steel **A**, longitudinal cross-sections of tested AER specimens were performed to characterize damage by void growth to coalescence. For loading along  $T$ , all the observed coalescence situations occurred by void impingement. Figure 6(a) illustrates a *knifedge* separation between two cavities as being the final stage of a coalescence by internal necking (Thomason, 1985b). For  $L$ -loading, elongated voids tend to

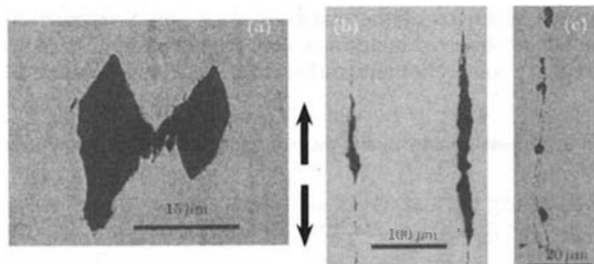


**Fig. 6 Typical coalescence modes observed in steel A (a)  $T$ -loading (b) and (c)  $L$ -loading. Arrows indicate the loading direction.**

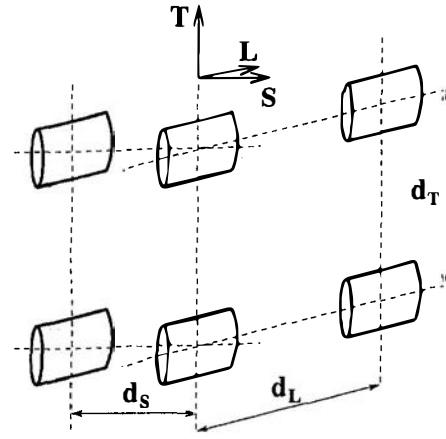


**Fig. 7 Schematic representation of MnS inclusions distribution in steel A**

impinge along the vertical direction as illustrated in Fig. 6(b) and (c). The situation in the micrograph Fig. 6(b) is observed at the center of the specimen where the stress triaxiality is the highest. Clearly, the coalescence mode depends on the loading direction. One should note however that, whatever the loading direction, final failure in a notched bar occurs by the propagation of a macroscopic crack initiated at the center of the specimen.

## 4.2 Finite Element Simulation

**Input Data.** In this section, we try to predict the failure of AER specimens in steel **A** using models accounting for inclusion spacing. The Gurson model is used together with critical porosities inferred from coalescence models ( $\mathcal{L}$ ) and ( $\mathcal{PL}2$ ). Accounting for void shape would require additional development of our finite element software. For that purpose, further assumptions have to be made to use models ( $\mathcal{L}$ ) and ( $\mathcal{PL}2$ ) restricted to axisymmetric void distributions, Fig. 1. We use a constant initial porosity characteristic of the material, equal to the volume fraction of inclusions  $f_v$  (Table 4). Here, the idea is to assume a  $\lambda_0^{(X)}$  value related to the tensile direction  $X$ . We adopt the following empirical extension to non-axisymmetric cases of the spacing ratio:  $\lambda_0^{(X)} = d_x/\sqrt{(d_y d_z)}$ , where  $d_x$  is the mean distance between inclusions along  $X$ -direction and  $Y-Z$  is the plane of normal  $X$ . Figure 7 illustrates a typical idealized distribution of MnS inclusions in the investigated materials. Based on preliminary observations, we assume that the ratios  $d_T/d_L$  and  $d_L/d_S$  in steel **A** are of the order of 4. Indeed, alignments of MnS inclusions are frequently observed along  $L$  direction, which suggests that 1) the inclusions are more closely packed in the thickness of the plate and 2)  $d_L < d_T$  although inclusions have larger  $L$  dimensions ( $D_L > D_T$ ).  $\lambda_0^{(X)}$  values inferred from this assumption are reported in Table 5. Critical porosities were calculated using the triaxiality values existing in the center of the specimen, for both coalescence models. For instance,  $\mathcal{F} = 0.8$  for AER10 specimens and  $\mathcal{F} = 1.4$  for AER2 specimens.  $f_c$  values are also reported on Table 5. After the onset of coalescence, the phenomenological modification of the Gurson model (Tvergaard and Needleman, 1984) was used

**Table 5 Inclusion spacing ratios and critical porosities  $f_c$  used in the finite element calculations.** (\*) corresponds to  $\lambda_0^{(T)} = 2$ .

Loading direction	Spacing ratio $\lambda_0^{(X)}$	specimen	$f_c$ (%)	
			( $\mathcal{PL}2$ )	( $\mathcal{L}$ )
$L$	$\lambda_0^{(L)} = 1$	AER10	1.74	2.3
		AER2	2.08	3.15
$T$	$\lambda_0^{(T)} = 8$	AER10	0.41	0.59
		AER2	0.3	0.47
$LT$	$\lambda_0^{(LT)} = 1.5$	AER10	1.31	1.4*
		AER2	1.39	1.52*

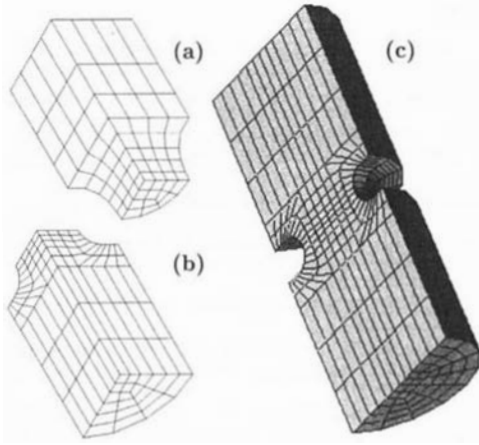


Fig. 8 Finite element meshes. (a) AER10; (b) AER2 for L- and T-loading; (c) AER2 for LT-loading

with  $f^* = f_c + \delta(f - f_c)$  where  $\delta = 8$ . However, results on AER specimens were found to be almost independent on the value of  $\delta$  for  $\delta > 10$ .

**Simulation.** Fully 3D calculations of AER specimens accounting for plastic anisotropy were made using ZéBuLoN7 software (Besson and Foerch, 1997). Quadratic quadrilaterals subintegrated elements with updated Lagrangian finite strain formulation were used. Figure 8 shows the meshes of two calculated specimens: a mildly notched one AER10 and a severely notched one AER2. In order for the elements in the minimal section to be roughly square at the initiation of fracture, the element size was  $0.5 \times 0.5 \times 0.25 \text{ mm}^3$ .

A recent theoretical extension of the Gurson criterion to the case of orthotropic materials (Benzerga et al., 1997) was used. Matrix yielding obeys Hill's criterion while the isotropic hardening law is fitted for L-direction.

**Results.** Results of finite element calculations for steel A are shown in Fig. 9. The mean stress (i.e., the load normalized by the initial minimal section) is plotted versus the mean strain  $\bar{\epsilon}$ . Calculations performed with a Mises isotropic plastic flow showed that the load is poorly predicted by the simulation. A better agreement was obtained when using Hill's criterion

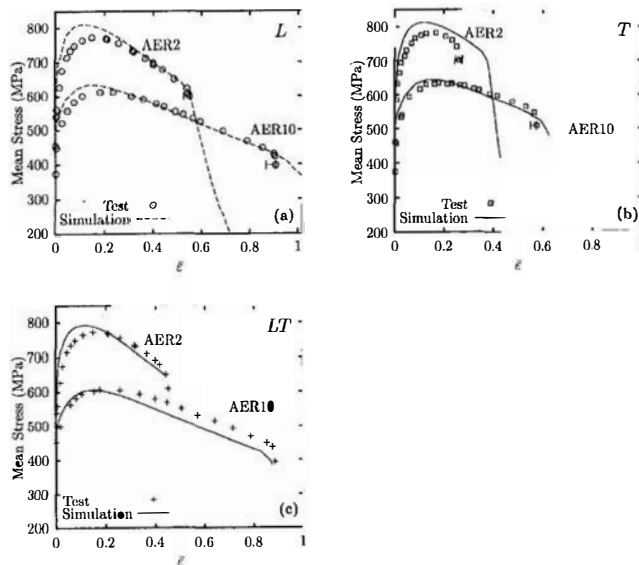


Fig. 9 Mean stress versus mean strain  $\bar{\epsilon}$ . Experimental and calculated curves. (a) L, (b) T, (c) LT.

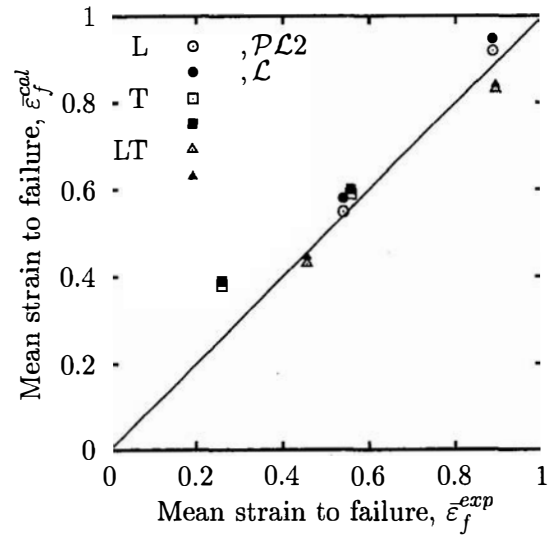


Fig. 10 Calculated ( $\bar{\epsilon}_f^{cal}$ ) and measured ( $\bar{\epsilon}_f^{exp}$ ) mean strains to failure

(Benzerga et al., 1997). However, Fig. 9 shows that numerical simulations tend to overestimate the load, in particular at high triaxialities. The results shown in Fig. 9 are those obtained using  $f_c$  values inferred from the plastic limit-load model (PL2). The correspondance between calculated and experimental responses is reasonable, whatever the loading orientation. It is worth emphasizing that no adjustment of micromechanical parameters is done; predicted critical porosities values are only used. These encouraging results strongly suggest that accounting for void spacing could, even partially, explain the anisotropic fracture properties of steel A.

Finally, Fig. 10 shows the correspondance between experimental and calculated mean strains to failure obtained using both models (L) and (PL2). Predictions of model (PL2) are closer to the experimental values. Nevertheless, poor results are obtained in T-loading when the triaxiality increases, Fig. 9(b). This suggests that the effect of inclusion shape, and not only particle spacing, remains central in anisotropic ductile fracture (Benzerga et al., 1998).

## 5 Concluding Remarks and Discussion

(1) From a practical point of view, the anisotropic ductile fracture evidenced in both materials A and B can be explained by synergistic effects of inclusion shape and inclusion spacing.

In this paper, the emphasis was laid on the inclusion spacing effect represented by the parameter  $\lambda_0$ . This effect was studied separately from the void shape effect since its influence is only on the onset of coalescence and not on the cavity growth stage. An approach was proposed to model the anisotropic ductile rupture by considering different coalescence loci in relation to loading direction. However, in spite of the good agreement between experimental and predicted results, we are aware of the numerous limitations of this approach. The most important is the void shape effect neglected in predictions of models (L) and (PL2). The observed discrepancy, in T-loading at high triaxiality, between experimental and calculated results is likely due to the inclusion shape effect. Indeed, the observed decrease in  $\bar{\epsilon}_f$  values with stress triaxiality, Table 3, is not well represented by the applied approach. Recently, inclusion shape effect on void growth was analyzed using a micromechanical model (Benzerga et al., 1998). It was shown that the decrease in ductility is actually more rapid when the macroscopic loading is perpendicular to the common axis of the voids. This is in agreement with the data of Table 3 for both steels A and B.

Further evidence of the influence of inclusion shape can be deduced from the comparison between the fracture properties

of steels **A** and **B**. Both of them contain comparable amounts of sulfur and manganese elements and have similar hardening exponents ( $\approx 0.13$ ). They essentially differ in the mean inclusion shape. Of course inclusions distributions may also be different. An attempt was made to predict  $\bar{\epsilon}_f$  in notched bars of steel **B** using different values of the spacing ratio parameter. No convenient values have been found using an estimation of  $\lambda_0^{(k)}$  from the material processing data (Lautridou and Pineau, 1981).

It is felt that if the differences in particle shape between both materials (Table 4) were properly taken into account, then a better agreement would be achieved, as suggested from the theoretical results given in Fig. 5. In a future work, we will use model ( $\mathcal{LP}3$ ) to perform finite element simulation of notched bars.

(2) From a theoretical point of view, two main ideas in the work on coalescence modeling should be underlined. The first one arises from the crucial role of stress triaxiality not only on void growth but also on coalescence. In addition, in both approaches ( $\mathcal{L}$ ) and ( $\mathcal{PL}2$ ), the idea of a deformation-induced cavitation inhomogeneity is introduced. This is expressed by the achievement of a plastic limit-load in the ligament between cavities (model ( $\mathcal{PL}2$ )) or by the rigidity of some compact zones that separate porous layers (model ( $\mathcal{L}$ )). A mathematical evidence of the theoretical equivalence of both approaches was made (Gologanu, 1997). The observed differences between both of them are mainly due to different geometrical assumptions.

In the present study, an attempt was made to investigate the effect of some microstructural parameters. The first metallurgical parameter investigated is the volume fraction of inclusions  $f_0$ . The obtained values of  $f_c$  lead to realistic values of ductility, in accordance with experimental results (Edelson and Baldwin, 1962). Moreover, the influence of the initial void distribution characterized by the particle spacing ratio  $\lambda_0$  was shown to be prevalent at high triaxialities where a relative insensitivity to  $f_0$  is evidenced. It was also shown that the corrections brought by the incorporation of the void shape effect are mainly useful for low and intermediate stress triaxialities. These results suggest that, for crack modeling, the most important metallurgical parameter is the void spacing. For low triaxiality however, the effect of void shape is crucial. The attempt to derive a unique critical porosity, for instance, through the simulation of a smooth specimen using classical models assuming spherical void growth is vain. Two reasons can be given: (1) in the general case, the critical porosity at coalescence evolves with stress state. (2) classical approaches based on the Gurson model lead to wrong predictions at triaxialities close to  $\frac{1}{3}$ .

It is worth noting that the effect of particle spacing has received less attention in the literature. This effect has been, in particular, studied in modeling crack initiation, see Rice and Johnson (1970), Lautridou and Pineau (1981), Garrison and Moody (1987b). The influence of the particle spacing itself instead of a dimensionless parameter, as defined here by  $\lambda$ , is questionable. Some elegant experimental studies (Garrison and Moody, 1987b; Garrison et al., 1997) have actually shown an effect of the void spacing itself. However, limitations in the correlation between fracture toughness and mean inter-particle distance in a plane perpendicular to the crack front have been underlined (Lautridou and Pineau, 1981). Clearly this indicates that further studies are necessary to show if only nondimensional distance parameters can be used to model coalescence in ductile fracture. In addition, in many materials, coalescence is driven by the formation of a second population of cavities leading to void-sheet mechanism. The models presented in this study do not strictly apply to this situation.

## Acknowledgments

This study has been supported by Gaz de France (GDF). R. Batisse and F. Curie from GDF are greatly acknowledged.

## References

- Batisse, R., Bethmont, M., Devesa, G., and Rousselier, G., 1988, "Ductile fracture of A508 C13 steel in relation with inclusion content: the benefit of the local approach of fracture and continuum damage mechanics," *Nuc. Eng. Design*, 105:113–120.
- Benzerga, A. A., Besson, J., and Pineau, A., 1997, "Modèle couplé comportement-encastrement ductile de tôles anisotropes," Peseux, B., Aubry, D., Pelle, J. P., and Touratier, M., editors, *Actes du Troisième Colloque National en Calcul des Structures*, pages 673–678. Presses Académiques de l'Ouest.
- Benzerga, A. A., Besson, J., Batisse, R., and Pineau, A., 1998, "Anisotropic ductile rupture," Brown, M. W., de los Rios, E. R., and Miller, K. J., editors, *12<sup>th</sup> European Conference on Fracture*, pages 715–720.ESIS, European Group on Fracture Publication.
- Beremin, F. M., 1981, "Cavity formation from inclusions in ductile fracture," *Met. Trans.*, 12A:723–731.
- Besson, J. and Foerch, R., 1997, "Large scale object oriented finite element code design," *Computer Methods in Applied Mechanics and Engineering*, 142:165–187.
- Brocks, W., Sun, D. Z., and Hömig, A., 1995, "Verification of the transferability of micromechanical parameters by cell model calculations with visco-plastic materials," *Int. J. Plasticity*, 11(8):971–989.
- Budiansky, B., Hutchinson, J. W., and Slutsky, S., 1982, "Void growth and collapse in viscous solids," Hopkins, H. G. and Sowell, M. J., editors, *Mechanics of Solids, The Rodney Hill 60th Anniversary Volume*, pages 13–45. Pergamon press.
- Doege, E., El-Dsoki, T., and Seibert, D., 1995, "Prediction of necking and wrinkling in sheet-metal forming," *J. Mat. Proc. Tech.*, 50:197–206.
- Edelson, B. I. and Baldwin, W. M. J., 1962, "The effect of second phases on the mechanical properties of alloys," *Trans. ASM*, 55:238.
- Franklin, A. G., 1969, "Comparison between a quantitative microscope and chemical methods for assessment of non-metallic inclusions," *J. of The Iron and Steel Institute*, 12:181–186.
- Garrison, W. M., and Moody, N. R., 1987a, "Ductile Fracture," *J. Phys. Chem. Solids*, 48(11):1035–1074.
- Garrison, W. M. and Moody, N. R., 1987b, "The influence of inclusion spacing and microstructure on the fracture toughness of the secondary hardening steel AF1410," *Metallurgical Transactions*, 18A:1257–1263.
- Garrison, W. M., Wojcieszynski, A. L., and Iorio, L. E., 1997, "Effects of inclusion distributions on the fracture toughness of structural steels," R. K. Mahidhara, A. B. Geltmacher, P. M. and Sadasananda, K., editors, *Recent Advances in Fracture*, pages 125–136. TMS.
- Gologanu, M., 1997, "Etude de quelques problèmes de rupture ductile des métaux," PhD thesis, Université Paris 6.
- Gologanu, M., Leblond, J.-B., and Devaux, J., 1994, "Approximate models for ductile metals containing non-spherical voids—case of axisymmetric oblate ellipsoidal cavities," *ASME JOURNAL OF ENGINEERING MATERIALS AND TECHNOLOGY*, 116:290–297.
- Gologanu, M., Leblond, J.-B., Perrin, G., and Devaux, J., 1997, *Continuum Micromechanics*, Recent extensions of Gurson's model for porous ductile metals. pp. 61–130, Suquet, P., ed. Springer-Verlag.
- Gurson, A. L., 1977, "Continuum theory of ductile rupture by void nucleation and growth: Part I—Yield criteria and flow rules for porous ductile media," *ASME JOURNAL OF ENGINEERING MATERIALS AND TECHNOLOGY*, 99:2–15.
- Koplik, J. and Needleman, A., 1988, "Void growth and coalescence in porous plastic solids," *Int. J. Solids Structures*, 24:835–853.
- Lautridou, J. C. and Pineau, A., 1981, "Crack initiation and stable crack growth resistance in a508 steels in relation to inclusion distribution," *Engineering Fracture Mechanics*, 15(1–2):55–71.
- Leblond, J.-B. and Perrin, G., 1991, "Analytical study of the coalescence of cavities in ductile fracture of metals," *Plasticity 3rd Symposium on Anisotropy and Localization of Plastic Deformation*, pages 233–236.
- Marini, B., Mudry, F., and Pineau, A., 1985, "Experimental study of cavity growth in ductile rupture," *Eng. Frac. Mech.*, 22:989–996.
- Mc Clintock, F. A., 1968, "A criterion for ductile fracture by the growth of holes," *ASME Journal of Applied Mechanics*, 35:363–371.
- Mudry, F., 1982, "Etude de la rupture ductile et de la rupture par clivage d'aciers faiblement alliés," PhD thesis, Doctorat d'état, Université de Technologie de Compiègne.
- Ottosen, N. S. and Runesson, K., 1991, "Properties of discontinuous bifurcation solutions in elasto-plasticity," *Int. J. Solids Structures*, 27:401–421.
- Pardoen, T., Doghri, I., and Delannay, F., 1998, "Experimental and numerical comparison of void growth models and void coalescence criteria for the prediction of ductile fracture in copper bars," *Acta Mater.*, 46(2):541–552.
- Perrin, G., 1992, "Contribution à l'étude théorique et numérique de la rupture ductile des métaux," PhD thesis, Ecole Polytechnique.
- Pineau, A., 1981, "Review of fracture micromechanisms and a local approach to predicting crack resistance in low strength steels," Francois, D., editor, *Advances in Fracture Research*, pages 553–577. Pergamon press.
- Ponte Castañeda, P., and Zaidman, M., 1994, "Constitutive models for porous materials with evolving microstructure," *J. Mech. Phys. Solids*, 42:1459–1495.
- Rice, J. R. and Johnson, M. A., 1970, *Inelastic behavior of solids*, The role of large crack tip geometry changes in plane strain fracture, pages 641–672. Mc Graw-Hill.
- Rice, J. R. and Tracey, D. M., 1969, "On the enlargement of voids in triaxial stress fields," *J. Mech. Phys. Sol.*, 17:201–217.

- Riks, E., 1979, "An incremental approach to the solution of snapping and buckling problems," *Int. J. Solids Structures*, 15:529-551.
- Rousselier, G., 1987, "Ductile fracture models and their potential in local approach of fracture," *Nuc. Eng. Design*, 105:97-111.
- Rudnicki, J. W. and Rice, J. R., 1975, "Conditions for the localization of deformation in pressure-sensitive dilatant materials," *J. Mech. Phys. Solids*, 23:371-394.
- Sovik, O. and Thaulow, C., 1997, "Growth of spheroidal voids in elastic-plastic solids," *Fatigue Fract. Engng. Mater. Struct.*, 20:1731-1744.
- Suquet, P., 1993, "On bounds for the overall potential of power law materials containing voids with arbitrary shape," *Mechanical Research Community*, 19:51-58.
- Thomason, P. F., 1968, "A theory for ductile fracture by internal necking of cavities," *J. Ins. Metals*, 96:360.
- Thomason, P. F., 1985a, "A three-dimensional model for ductile fracture by the growth and coalescence of microvoids," *Acta Metallurgica*, 33(6):1087-1095.
- Thomason, P. F., 1985b, "Three-dimensional models for the plastic limit-loads at incipient failure of the intervoid matrix in ductile porous solids," *Acta Metallurgica*, 33(6):1079-1085.
- Tvergaard, V., 1981, "Influence of voids on shear band instabilities under plane strain conditions," *Int. J. Frac.*, 17:389-407.
- Tvergaard, V. and Needleman, A., 1984, "Analysis of the cup-cone fracture in a round tensile bar," *Acta Metall.*, 32:157-169.
- Yamamoto, H., 1978, "Conditions for shear localization in the ductile fracture of void-containing materials," *Int. J. Frac.*, 14:347-365.
- Zhang, Z. L. and Niemi, E., 1994, "Analyzing ductile fracture using dual dilational constitutive equations," *Fat. Frac. Eng. Mater. Structures*, 17:695-707.